

## **SUPPLEMENTARY INFORMATION**

### **1. FACTORS AFFECTING GAS TRANSPORT IN SUBSEA PERMAFROST**

Even if thawing is the most considered parameter known to affect the continuity and permeability of permafrost hence allowing the migration of gas from deeper layer to the surface, other important factors need to be taken into consideration as discussed below.

#### **1.1. Physical factors**

When sediments freeze, a certain amount of pore water (depending on water salinity, type of sediments and temperature) remains unfrozen within frozen sediments. The physical properties of frozen grounds/sediments may be influenced significantly by this unfrozen water. For example, when temperature changes from  $-6.5$  to  $-2.8^{\circ}\text{C}$ , the content of unfrozen water increases by 22.3% (Khimenkov and Brushkov, 2006). It was shown that within frozen mineralized coarse sands, unfrozen water accumulates in the center of the pore space, forming a net of fissures, building an efficient transportation system within frozen sediments (Arenson and Segoy, 2006) This system enables the movement of gaseous and dissolved  $\text{CH}_4$  inside the frozen permafrost (predominantly consisted of sandstone and gravel) as it has been demonstrated on Barrow Point (Alaska)(McCarthy et al., 2004).

On a larger scale, the hydraulic system also plays an important role. It represents the layers of mineralized water incorporated above, within and beneath permafrost – so called supra-permafrost, intra-permafrost and sub-permafrost ground water, respectively. The salinity of this cryogenic groundwater usually ranges between 10 and 300psu, in which freezing is prevented by freezing-point depression due to the dissolved-solids content of the pore water (Gilichinsky et al., 2007)in most cases very high as it often includes brines resultant from the freezing of marine sediments. These water layers are usually connected to each other to build a multi-level transport system and allowing gases and geo-fluids to migrate upwards and to be released to the water column through the subsea permafrost (Biggar et al., 1998). The hydraulic system serves as well to connect the deep permafrost to the surface enhancing the development of taliks with a network of mechanical discontinuities existing within the permafrost into an integrated transportation system for ascending gases and geofluids (Makogon et al., 2007).

#### **1.2. Seasonal variations**

Since seasonal variations in temperature in Arctic regions are very large, they affect frozen soils/sediments by causing alternations of compression and stretching of frozen grounds. This leads, with time, to the development of numerous cracks filled with water and it results in the formation of cuneiform (wedge-like) shapes of ice inclusions in permafrost body. This mechanism was suggested to be responsible for the observed predominance of wedge-like type of ice within permafrost body widely spread

49 on the Arctic coasts. Such an extensive network of cracks in the structure of  
50 frozen rocks serves as well to provide gas migration paths for ascending  
51 gases and geofluids (Romanovskii et al., 2000).

52

### 53 **1.3. Destabilization of gas hydrate deposits**

54

55 Another group of factors influencing gas transport within subsea  
56 permafrost can be associated to the destabilization of gas hydrates deposits  
57 (e.g. Clenell et al., 1999, Romanovskii et al., 2005, Nicolisky et al., 2012).  
58 The thermal and pressure conditions determining the stability/instability of the  
59 gas hydrates are very specific (Shakhova et al., 2009). When shallow shelf  
60 hydrates destabilize, overly pressured gas from the decaying hydrates  
61 accumulates between the lower boundary of permafrost and the upper  
62 boundary of hydrate stability (Naudts et al., 2006, Sergienko et al., 2012).  
63 This over-pressurized gas front moves both horizontally and vertically  
64 following the unconformities and discontinuities of the permafrost body  
65 (Cramer et al., 2005). Within developing taliks, this front can also constitute  
66 gas migration pathways of high capacity (Osterkamp et al., 1985, Frederick et  
67 al., 2014).

68

## 69 **2. DEEP CORE LITHOLOGY**

70

71 The major differences in the lithology of the deep cores drilled in 2011  
72 and 2013 are the thickness and the origin of the Holocene age sediment. In  
73 the background core, Holocene age marine sediments compose the upper  
74 5.5m, they represent disperse pelite-aleurite deposits predominantly of  
75 alluvial origin, which are accumulations of river-derived matter formed in  
76 coastal marine conditions with high rates of sediment accumulation (Fig.S1).  
77 Holocene sediments are underlain with terrestrial accumulations (5.8m to  
78 52.3m) of late Pleistocene age, which are represented by consolidated  
79 aleuro-sands inter-layered by fine-grained aleurite accumulations with  
80 inclusions of pebbles and wood remains.

81

82 The other deep cores were drilled in 2013 near the Muostakh Island. In  
83 the IID-13 and IIID-13 cores, the Holocene age sediments represent only the  
84 upper 0.5m and consist of remains of the coastal ice-complex (IC or Yedoma)  
85 of Muostakh Island. This area represents a former part of the coastal alluvial  
86 plain, upper part of which is composed of IC that thaws very fast during the  
87 last century. Sediment morphology reflects the nature of the sediments: fine-  
88 grained sand-aleurite-pelite is interlayered with gravel-pebble material with  
89 inclusions of wood remains and plant debris.

89

90 Sediment core VD-13 stands out of all the other cores drilled in 2013.  
91 Its morphological structure is different as its frozen fraction is presented by  
92 sands interlayered by gravel-pebble accumulations. It is known that coarse  
93 sands even frozen remain permeable for gases as within their frozen  
94 structure fissures form that allow pore water to remain unfrozen; these  
95 fissures were suggested to be serving as gas migration paths (Arenson and  
96 Segó, 2006) as discussed in section 1.1. Note, that other drilling data  
obtained in the study area have shown that at water depth ~ 11m, the upper

97 57m sediment is entirely unfrozen with typical temperature about 0 degC  
98 (Shakhova et al., 2014). Downward extrapolation of the temperature curve  
99 together with permafrost modeling show the existence of open taliks in the  
100 Buor Khaya Bay where all samples were taken. Similar field and modeling  
101 results were obtained for the Dmitry Laptev Strait (Shakhova et al., 2009;  
102 Nicolsky and Shakhova, 2010). This means that hydrocarbons from deeper  
103 strata could migrate through these migration paths.

104

### 105 **3. INTERPRETATION OF THE <sup>14</sup>C-CH<sub>4</sub> RESULTS**

106

107 The observation of unexpectedly high <sup>14</sup>C values for the ID-11  
108 background core and water samples from the SE needs further discussion.  
109 As explained in the main text, <sup>14</sup>C values >200pmC do not exist in nature for  
110 any carbonaceous material including CH<sub>4</sub>, even not for the peak of surface  
111 nuclear bomb tests of the mid-20<sup>th</sup> century. We assume that a local  
112 anthropogenic nuclear contribution is the most likely explanation for our  
113 elevated radiocarbon levels, which is justified in this section.

114 In the ID-11 background sediment, the higher <sup>14</sup>C values correspond to  
115 the lower CH<sub>4</sub> concentrations. That implies a possible mixture between an old  
116 CH<sub>4</sub> source and a background highly enriched in <sup>14</sup>C. A Keeling plot shows  
117 that the highly enriched <sup>14</sup>C contribution is relatively small in terms of CH<sub>4</sub>  
118 quantity and that the main CH<sub>4</sub> substrate is relatively old (Fig. S2). For the  
119 hotspot sites, where CH<sub>4</sub> concentrations are larger, no mixture with a  
120 “younger” source is identified. All data points are showing very low <sup>14</sup>C  
121 (<1.5pmC) so the main CH<sub>4</sub> substrate at these sites is clearly of Pleistocene  
122 age. Note that all points of the IID-13 core were below the analytical detection  
123 limit of 0.8pmC hence no conclusions could be drawn from the Keeling plot of  
124 this core.

125 The very high <sup>14</sup>C values >200pmC may either originate from “in-situ”  
126 cosmogenic or nuclear production of radioactive CH<sub>4</sub> or its substrate.  
127 Enhanced <sup>14</sup>C has been found in meteorites (Firemann, 1978) and can be  
128 produced at the surface of ice sheets (Baudin et al., 1973), but in both cases,  
129 the quantity of <sup>14</sup>C formed is very small compare to what we observed in the  
130 BKB and SE sediment and water samples. Nuclear production of <sup>14</sup>C involves  
131 formation by neutron activation as consequence of a nuclear chain reaction,  
132 which may either take place naturally or artificially. The only place on Earth,  
133 where nuclear fission has occurred naturally, was reported to be occurring  
134 about 1.7 billion years ago in Oklo, Gabon (Nuclear Wastes in the Arctic  
135 report, 1995). However, such natural reactors cannot be active anymore  
136 today, as the relative abundance of fissile <sup>235</sup>U has now decayed below that  
137 required threshold for a sustainable nuclear reaction chain.

138 The Arctic Ocean has been used as a disposal area for radioactive  
139 wastes (Nuclear Wastes in the Arctic report, 1995, Johnson-Pyrtle and Scott,  
140 1991) hence we believe that anthropogenic nuclear contamination is the most  
141 likely explanation for these <sup>14</sup>C-enriched CH<sub>4</sub> background contribution. Similar  
142 cases but with slightly lower values have been observed in gas samples from  
143 marine basins along the Californian coast (Kessler et al., 2008). The authors

144 assumed nuclear plant effluents as being the most likely explanation for these  
145 unexpected data.

146 We exclude a possible contamination during sampling, extraction and  
147 analysis, because no radioactive tracers were used during the sampling  
148 expeditions. The samples affected by enriched  $^{14}\text{C}$  values were not sampled  
149 in a similar manner. The sediment samples were drilled from the ice in 2011  
150 while the SE water samples were sampled in 2012 from a ship together with  
151 other water and surface sediment samples showing no enrichment in  $^{14}\text{C}$   
152 values. For the rest of the sampling and analysis process, all samples were  
153 handled in a similar way and measured in a random order, but only samples  
154 from these two specific locations show highly enriched  $^{14}\text{C}$  values. None of  
155 the reference and blank measurements was abnormal either.

156

157

158

159

## SUPPLEMENTARY REFERENCES

- 160  
161  
162 Arenson, L. U. and Segoy, D., C.: The Effect of Salinity on the Freezing of  
163 Coarse-Grained Sands, *Can. Geotech. J.* 43, 325–337, 2006.  
164  
165 Baudin, G., Blain, C., Hagemann, R., Kremer, M., Lucas, M., Merlivat, L.,  
166 Molina, R., Nieff, G., Prost Marechal, P., Regnaud, F. & Roth, E.: Quelques  
167 données nouvelles sur les reactions nucléaires en chaine que se sont  
168 produites dans le gisement d’Oklo, *C.R. Acad. Sci. Paris*, 275D, 2291, 1973.  
169  
170 Biggar, K. W., Haidar, S., Nahir, M., and Jarrett, P. M.: Site Investigation of  
171 Fuel Spill Migration into Permafrost, *ASCE J. Cold Regions Eng.* 2, 84–104,  
172 1998.  
173  
174 Clennell, M. B., M. Hovland, J. S. Booth, P. Henry, and W. J. Winters,  
175 Formation of natural gas hydrates in marine sediments: 1. Conceptual model  
176 of gas hydrate growth conditioned by host sediment properties, *J. Geophys.*  
177 *Res.*, 104(B10), 22985–23003, 1999.  
178  
179 Cramer B. and Franke, D.: Indications for an Active Petroleum System in the  
180 Laptev Sea, NE Siberia, *J. Petroleum Geol.* 28, 369–384, 2005.  
181  
182 Firemann, E. L.: Carbon-14 in lunar soil and in meteorites, *Proc. Lunar Planet.*  
183 *Sci. Conf.* 9<sup>th</sup>, 1647-1654, 1978.  
184  
185 Fireman, E. L. & T. L. Norris, Ages and composition of gas trapped in Allan  
186 Hills and Byrd core ice, *Earth and Planetary Science Letters*, 60, 339-350,  
187 1982.  
188  
189 Frederick, J. M., and B. A. Buffett: Taliks in relict submarine permafrost and  
190 methane hydrate deposits: Pathways for gas escape under present and future  
191 conditions, *J. Geophys. Res. Earth Surf.*, 119, 106–122, 2014.  
192  
193 Gilichinsky, D., Rivkina, E., Bakermans, C., Shcherbakova, V., Petrovskaya,  
194 L., Ozerskaya, S., Ivanushkina, N., Kochkina, G., Laurinavichus, K.,  
195 Pecheritsina, S., Fattakhova, R., and Tiedje, J.M.: Biodiversity of cryopegs in  
196 permafrost. *FEMS Microbiol. Ecol.* 53, 117–128, 2005.  
197  
198 Johnson-Pyrtle, A. and Scott, M.R.: Distribution of <sup>137</sup>Cs in the Lena River  
199 Estuary-Laptev Sea System, *Marine Pollution Bulletin* Vol. 42, No. 10, pp.  
200 912-926, 2001.  
201  
202 Kessler, J. D., Reeburgh, W.S., Valentine, D.L., Kinnaman, F.S., Peltzer, E.T.,  
203 Brewer, P.G., Southon, J. & Tyler, S.C.: A survey of methane isotope  
204 abundance (<sup>14</sup>C, <sup>13</sup>C, <sup>2</sup>H) from five nearshore marine basins that reveals  
205 unusual radiocarbon levels in subsurface waters, *J. Geophys. Res.*, 113,  
206 C12021, 2008.  
207

208 Khimenkov, A. N., and Brushkov, A. V. Introduction to Structural Cryology.  
209 Nauka, Moscow, pp. 279, 2006.  
210

211 Makogon, Y. F., Holditch, S. A., and Makogon, T. Y.: Natural Gas Hydrates: A  
212 Potential Energy Source for the 21st Century, *J. Petroleum Sci. Engineering*  
213 56, 14–31, 2007.

214 McCarthy, K., Walker, L., and Vigoren, L.: Subsurface Fate of Spilled  
215 Petroleum Hydrocarbons in Continuous Permafrost, *Cold Regions Sci.*  
216 *Technol.* 38, 43–54, 2004.  
217

218 Naudts, L., Greinert, J. and Artemov, Y. et al.: Geological and Morphological  
219 Settings of 2778 Methane Seeps in the Dnepr Paleo-Delta, Northwestern  
220 Black Sea, *Marine Geol.* 227, 177–199, 2006.  
221

222 Nicolsky, D., Romanovsky, V. E., Romanovskii, N. N., Kholodov, A. L.,  
223 Shakhova, N. E., & Semiletov, I. P.: Modeling sub-sea permafrost in the East  
224 Siberian Arctic Shelf: The Laptev Sea region. *J. Geophys. Res.*, 117, F03028,  
225 2012.  
226

227 Nuclear Wastes in the Arctic: An Analysis of Arctic and Other Regional  
228 Impacts from Soviet Nuclear Contamination, OTA-ENV-623 (Washington, DC:  
229 U.S. Government Printing Office, September), 1995.  
230

231 Osterkamp, T. E. and Harrison, W. D.: Sub-Sea Permafrost: Probing, Thermal  
232 Regime, and Data Analyses, 1975–1981, Summary Report (Geophys. Inst.,  
233 Univ. of Alaska Fairbanks), 1985.  
234

235 Romanovskii, N. N., Hubberten, H.-W., Gavrilov, A.W. et al.: Thermokarst and  
236 Land-Ocean Interaction, Laptev Sea Region, Russia, *Permafrost Periglac.*  
237 *Processes* 11, 137–152, 2000.  
238

239 Romanovskii, N. N., Hubberten, H.-W., Gavrilov, A. V., Eliseeva, A. A., &  
240 Tipenko, G. S.: Offshore permafrost and gas hydrate stability zone on the  
241 shelf of East Siberian Seas. *Geo-Mar. Lett.*, 25, 167-182, 2005.  
242

243 Sergienko, V. I., Lobkovskii, L. I., Semiletov, I. P., Dudarev, O. V., Dmitrievskii,  
244 N. N., Shakhova, N. E., Romanovskii, N. N., & Bukhanov, B.: The  
245 Degradation of Submarine Permafrost and the Destruction of Hydrates on the  
246 Shelf of East Arctic Seas as a Potential Cause of the “Methane Catastrophe”:  
247 Some Results of Integrated Studies in 2011. *Dokl. Earth Sci.*, 446(1), 1132-  
248 1137, 2012.  
249

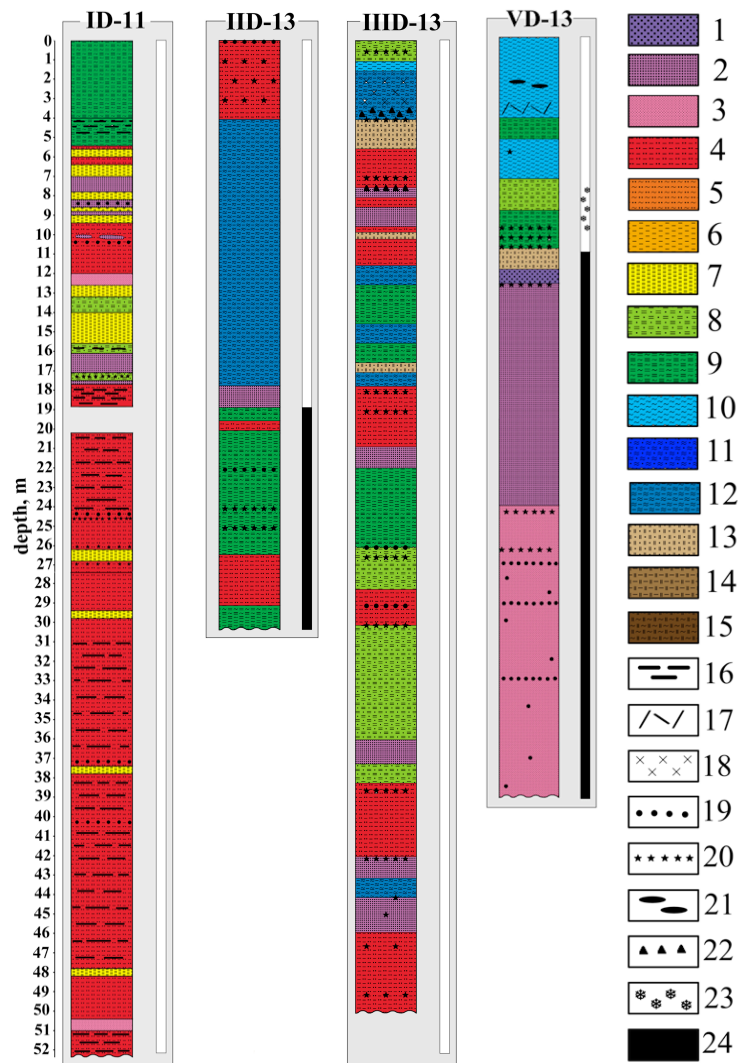
250 Shakhova, N.E., Sergienko, V.I., Semiletov, I.P.: The contribution of the East  
251 Siberian Arctic Shelf in to the modern methane cycle, *Herald of the RAS*, Vol.  
252 79 (3), 237–246., 2009.  
253  
254  
255

256

257

258  
 259  
 260  
 261  
 262  
 263  
 264  
 265

## SUPPLEMENTARY FIGURES

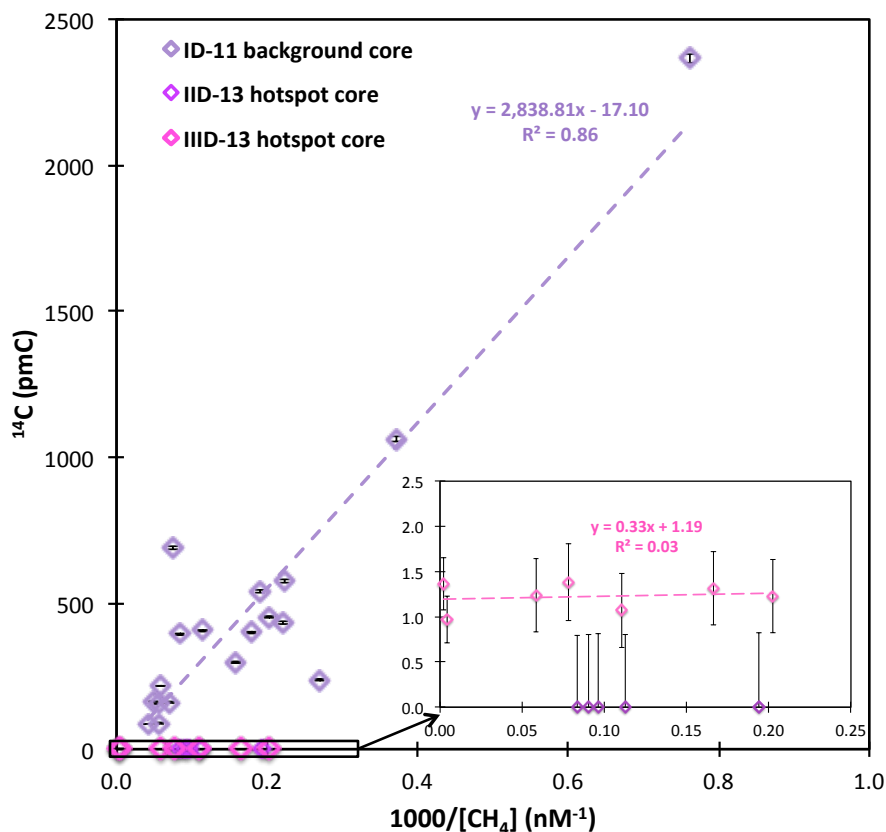


266  
 267  
 268  
 269  
 270  
 271  
 272  
 273  
 274  
 275  
 276  
 277  
 278  
 279  
 280

Figure S1. Morphological structure of the sediment cores extracted from boreholes drilled in 2011 (ID-11) and 2013 (IID-13, IIID-13 and VD-13). Lithological structure: 1 - coarse sand, 2- medium-grained sand, 3 - fine-grained sand, 4 - aleuro-sand, 5 - pelite-sand, 6 - coarse-grained aleurite, 7 - fine-grained aleurite, 8 - sand-aleurite, 9 - pelite-aleurite 10 - pelite, 11 - sand-pelite, 12 - aleuro-pelite, 13 - sand-mictite, 14 - aleuro-mictite, 15 - pelite-mictite; Texture characteristics: 16 - horizontal layered texture, 17 - vertical fine banded texture, 21 - horizontal lense-like texture; Diagenesis characteristics: 18 - H<sub>2</sub>S presence; Inclusions: 19 - gravel-pebble products, 20 - plant debris, 22 - shell detritus; Cryogenic structure: 23 - ice-lenses/lenticular-layered cryostructure, 24 - frozen ground with massive (in sands) and micro-lenticular cryostructures (shown vertically along the cores).

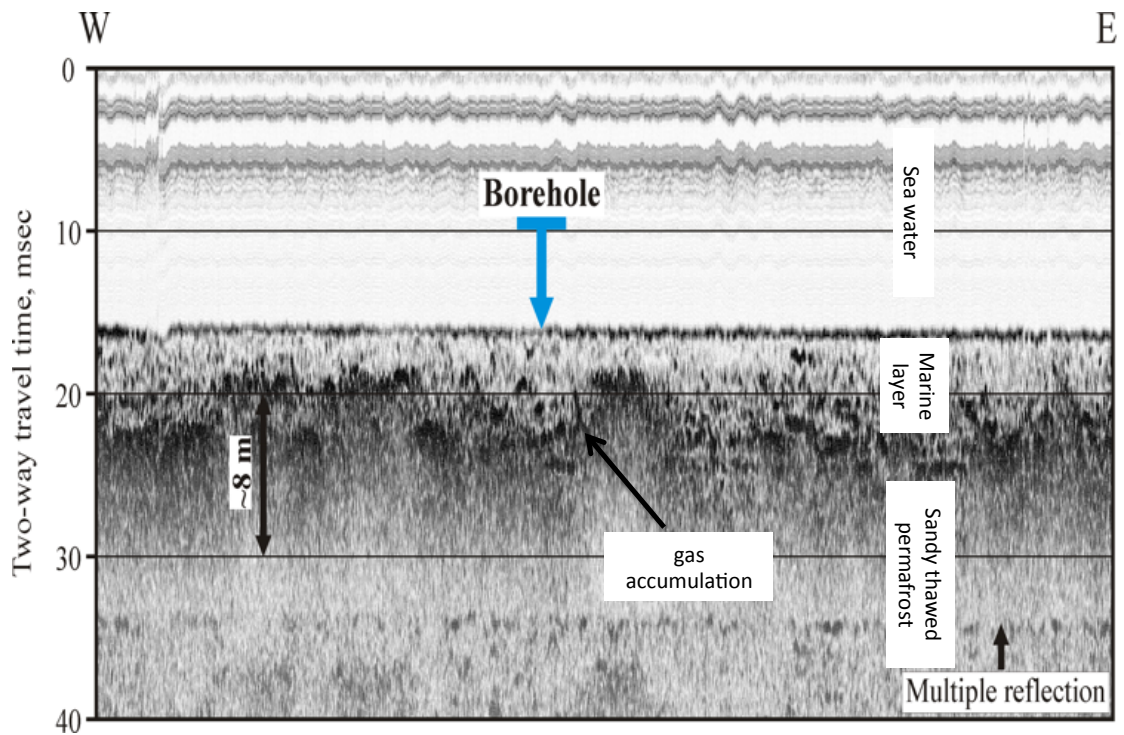


281  
282



283  
284  
285  
286  
287  
288  
289  
290  
  
291  
292  
293  
294  
295  
296  
297  
  
298  
299  
300  
301  
302

Figure S2: Keeling plot: inverse CH<sub>4</sub> concentration versus <sup>14</sup>C data for sediment samples in the partially thawed subsea permafrost. The diamonds are “deep” core sediment data and the dashed lines represent the linear regressions for the ID-11 (purple) and IID-13 (pink) cores. All values of the IID-13 core are close to zero so no linear regression line is depicted for this core. The intersections with the y-axis correspond to the <sup>14</sup>C pmC values of the main CH<sub>4</sub> substrate.



303  
304  
305

Figure S3: Acoustic profile of the borehole of the ID-11 drilling site. Darker areas represent changes in density between the different horizontal layers (Sergienko et al., 2012).